

# NOCTURNAL LOW-LEVEL JET CHARACTERISTICS OVER KANSAS DURING CASES-99

R. M. BANTA<sup>1,\*</sup>, R. K. NEWSOM<sup>2</sup>, J. K. LUNDQUIST<sup>3</sup>, Y. L. PICHUGINA<sup>2</sup>, R. L. COULTER<sup>4</sup> and L. MAHRT<sup>5</sup>

<sup>1</sup>*Environmental Technology Laboratory/NOAA, 325 Broadway, Boulder, Colorado 80305, U.S.A.;*

<sup>2</sup>*Cooperative Institute for Research in the Atmosphere, Ft. Collins, Colorado, U.S.A.;* <sup>3</sup>*Program in Atmospheric and Oceanic Sciences, University of Colorado, Boulder, U.S.A.;* <sup>4</sup>*Argonne National Laboratory, IL, U.S.A.;* <sup>5</sup>*College of Oceanic and Atmospheric Sciences, Oregon State University, Corvallis, U.S.A.*

(Received in final form 24 December 2001)

**Abstract.** Characteristics and evolution of the low-level jet (LLJ) over southeastern Kansas were investigated during the 1999 Cooperative Surface-Atmosphere Exchange Study (CASES-99) field campaign with an instrument complement consisting of a high-resolution Doppler lidar (HRDL), a 60-m instrumented tower, and a triangle of Doppler mini-sodar/profiler combinations. Using this collection of instrumentation we determined the speed  $U_X$ , height  $Z_X$  and direction  $D_X$  of the LLJ. We investigate here the frequency of occurrence, the spatial distribution, and the evolution through the night, of these LLJ characteristics. The jet of interest in this study was that which generates the shear and turbulence below the jet and near the surface. This was represented by the lowest wind maximum. We found that this wind maximum, which was most often between 7 and 10 m s<sup>-1</sup>, was often at or just below 100 m above ground level as measured by HRDL at the CASES central site. Over the 60-km profiler-sodar array, the topography varied by ~100 m. The wind speed and direction were relatively constant over this distance (with some tendency for stronger winds at the highest site), but  $Z_X$  was more variable.  $Z_X$  was occasionally about equal at all three sites, indicating that the jet was following the terrain, but more often it seemed to be relatively level, i.e., at about the same height above sea level.  $Z_X$  was also more variable than  $U_X$  in the behaviour of the LLJ with time through the night, and on some nights  $U_X$  was remarkably steady. Examples of two nights with strong turbulence below jet level were further investigated using the 60-m tower at the main CASES-99 site. Evidence of TKE increasing with height and downward turbulent transport of TKE indicates that turbulence was primarily generated aloft and mixed downward, supporting the upside-down boundary layer notion in the stable boundary layer.

**Keywords:** CASES-99, Lidar, Low-level jet, Nocturnal boundary layer, Stable boundary layer, Wind profiles.

## 1. Introduction

One of the most important processes in the evening boundary-layer transition over relatively flat terrain is the decoupling the flow just above the surface from surface friction, as a result of cooling at the ground. This decoupling disrupts the daytime

\* E-mail: robert.banta@noaa.gov



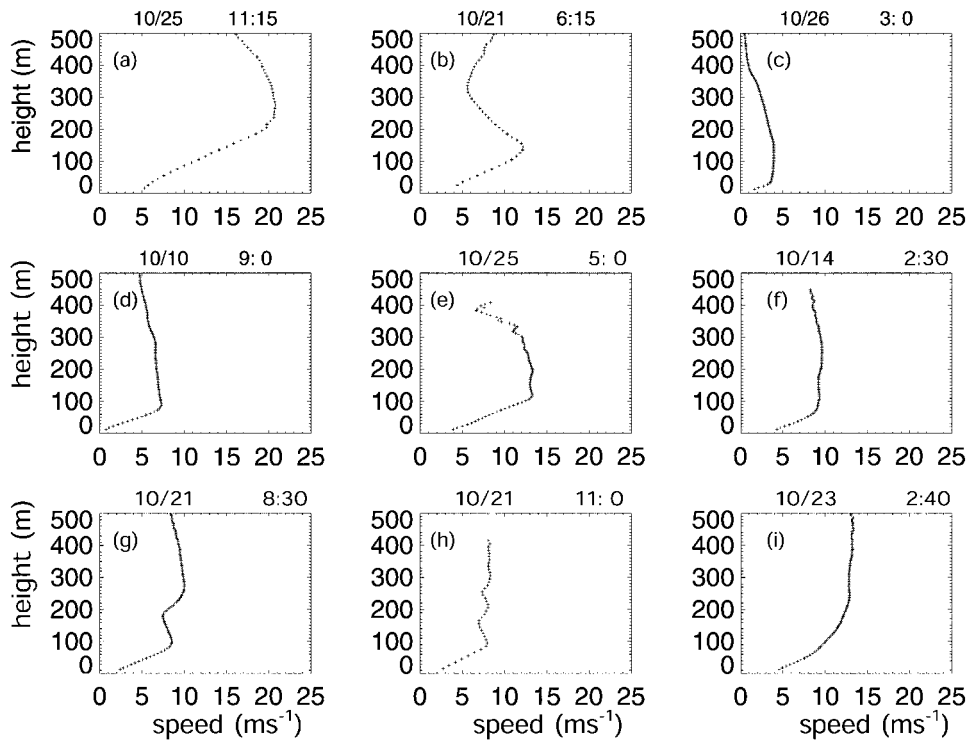


Figure 1. Sample LLJ profiles either from HRDL vertical-slice scans or from conical (VAD) scans. The lowest wind-speed maximum in each case except the last one was classified as a LLJ in this study. The last profile was not classified as a LLJ.

balance of forces in the horizontal and produces acceleration of the flow above the atmospheric surface layer in a manner well described by Blackadar (1957). The acceleration produces a layer of high-momentum air – extensive in the horizontal but shallow in the vertical – which often exhibits a maximum or nose in the vertical profile of the horizontal wind (see Figures 1a, b). This maximum has been called a low-level jet (LLJ). The dynamics of these flows, and their relationship to inertial oscillations, have been described by Blackadar (1957), Thorpe and Guymer (1977), Andreas et al. (2000), and Lundquist (2000).

LLJs are regular features of the nighttime stable boundary layer (SBL) during undisturbed conditions over non-mountainous terrain. They are important for a variety of applications, including wind energy and nocturnal transport of atmospheric quantities. For example, Banta et al. (1998) showed that transport by the nocturnal LLJ has an important role in the fate of urban-generated pollutants during a multi-day air-pollution episode. Indirectly, LLJs – especially those that form below 200 m above ground level (AGL) – are also important for generating shear between the level of the jet and the earth's surface, and this shear is likely to have a role in controlling fluxes between the surface and atmosphere. This connection

is potentially significant, because current-generation numerical weather prediction (NWP) models do not predict properties of these low LLJs very well. Mesoscale models, which may have sufficient vertical resolution to explicitly simulate these LLJs, have difficulty predicting their direction and strength, presumably because of crude representation of subgrid mixing in stable conditions. Larger-scale models, which have coarser vertical resolution, are incapable of simulating LLJs explicitly, and LLJ effects are not currently part of any parameterization schemes in these models. A better representation of LLJ-related processes in such models thus should improve their performance during the nighttime portion of the diurnal cycle.

The term LLJ has been used to refer to any low-level speed maximum in the vertical profile of the wind, and LLJ's can be produced by a number of mechanisms, which has led to ambiguity in the usage of this term in the literature. For example, density currents (including synoptic cold fronts, thunderstorm gust fronts, drainage-flow fronts, sea-breeze fronts, etc.) have an LLJ profile in the cold-air layer behind the front (Bowen, 1996; Droegemeier and Wilhelmson, 1987; Darby et al., 2002). Similarly, Whiteman et al. (1997) found in their LLJ climatology that most wind maxima that fit their criteria for an LLJ *and* had a northerly component were post-cold-frontal jets (and therefore large-scale density currents). LLJ climatologies show a small percentage of LLJ's occurring during daylight hours, and these would not be due to the Blackadar mechanism. Even nocturnal LLJs can have different causes and scales of geostrophic pressure gradients. For example, in the nocturnal LLJ of the Great Plains of the United States (Hoecker, 1963; Bonner, 1968; Mitchell et al., 1995; Frisch et al., 1992; Zhong et al., 1996; Whiteman, 1997), which has been extensively studied because of its impact in contributing to severe weather occurrence (Stensrud, 1996), the relevant pressure gradient has been ascribed either to baroclinity due to the sloping terrain or to the synoptic gradient associated with the Bermuda high-pressure system, either of which would produce a wind from a southerly direction. We note that these deeper LLJs have been successfully simulated with mesoscale models (Zhong et al., 1996).

In the present study we are concerned with the nocturnal LLJ that has a role in generating shear and turbulence between the level of maximum wind speed  $Z_X$  and the earth's surface, thus influencing, and sometimes probably controlling, surface-atmosphere exchange at night. Hence, we are interested in the lowest LLJ maximum that forms due to Blackadar's mechanism. The southeastern Kansas dataset that we are using for this study typically showed a single-level jet maximum, but many instances of multiple LLJ maxima also occurred (Figure 1). Even more significantly,  $Z_X$  for this site was frequently at or below 100 m above ground level (AGL). This level is below the minimum range of current-generation radar wind profilers, including the boundary-layer systems (900–1000 MHz), and thus these jets are undetectable by such instruments. Instrument capability is an important aspect of the nocturnal LLJ problem, and we address this issue later in the study.

The instrumentation used in this study included 915-MHz profilers, mini sodars, a 60-m meteorological tower, and the High-Resolution Doppler Lidar (HRDL) developed and deployed by the Environmental Technology Laboratory (ETL) of the National Oceanic and Atmospheric Administration (NOAA). Previous studies of nocturnal LLJs have been handicapped by coarse sampling in space and time, as pointed out by Whiteman et al. (1997), Lundquist (2000), and others. Profiles taken by HRDL in the present study were available at time intervals of  $\lesssim 1$  min with vertical resolutions of  $\lesssim 10$  m for a significant portion of the nights investigated, allowing the evolution of the nocturnal LLJ to be described in unprecedented detail. Grund et al. (2001) had previously shown HRDL to be ideally suited to studying the LLJ (see their Figure 9).

The purpose of the present study is to describe the characteristics, including speed, height, and direction, of LLJs observed during CASES-99. We use the datasets to determine the distributions of the frequency of occurrence of these characteristics, their spatial variability, and their behaviour as a function of time through the night. We show examples of the relationship between LLJ evolution and near-surface turbulence generation and mixing, which have been shown to be important consequences of LLJ formation (Smedman, 1988; Mahrt, 1999).

## 2. Instrumentation and Analysis Procedures

The Cooperative Surface-Atmosphere Exchange Study field campaign of October 1999 (CASES-99) was an intensive study of the nocturnal stable boundary layer (SBL). Poulos et al. (2002) describe the objectives, instrumentation, and venue in detail. CASES itself is a multi-year, interdisciplinary study of meteorological and hydrological processes in the Walnut River watershed in southeast Kansas, just east of Wichita. The backbone of CASES is a long-term deployment by Argonne National Laboratory (ANL) of 915-MHz radar wind profilers with minisodars and other instrumentation, including surface mesonet stations, called the Atmospheric Boundary Layer Experiments (ABLE) array (LeMone et al., 2000). ABLE includes a triangle of sodar/profiler sites surrounding the CASES-99 main site near the town of Leon, where HRDL was located at an elevation of 434 m MSL (scanner height). These sodar/profilers were at the following locations (see Figure 2). Beaumont (BEA), in the eastern portion of the watershed, is the highest station at an elevation of 460 m MSL. The northwestern site, Whitewater (WHI), has an elevation of 420 m. The southern Oxford (OXF) site is the lowest of the three at an elevation of 360 m MSL. More detailed maps of the main site are given in Poulos et al. (2002).

The official time for the CASES-99 project was the Universal Time Coordinate (UTC). An advantage of using UTC besides the absence of ambiguity over daylight vs. standard time, is that, because sunset occurred just before 0000 UTC, the date is the same for the entire night, instead of changing halfway through. Thus, UTC time represents the approximate number of hours after sunset. The basic time for

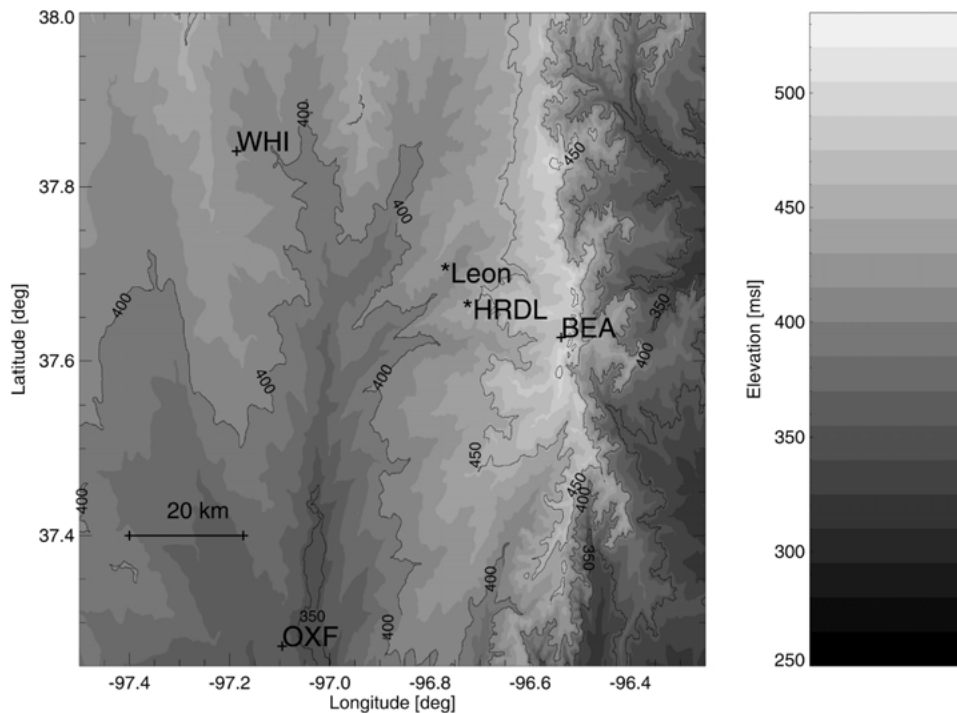


Figure 2. Topographic map of the study area showing HRDL location at the CASES-99 main site (black star) near Leon KS, and the locations of the three sodar/profiler sites (+). Lightest shading indicates high terrain of the Flint Hills running north-south near BEA, and dark shaded topography in middle indicates the valley of the Walnut River.

this paper will be UTC, but we note that a drawback is that having a reference to local hour would be lost for this study, in which the diurnal cycle is important. Therefore, we also include Central Standard Time (CST), which is 6 h behind UTC, in our references to time. We chose CST as the appropriate local time even though Kansas was on daylight savings time, because CST is closer to the solar diurnal cycle.

During each night of CASES-99, at least four and sometimes more than 20 rawinsondes were launched from various sites within the CASES-99 instrument array. These rawinsondes rely on a connection with Global Positioning System (GPS) satellites for position-finding and wind-finding. Of the 238 nocturnal (0000–1400 UTC) soundings taken during CASES-99, 165 lost their connection with the satellites upon launch, and thus were unable to provide winds in the lowest 100 m at least (Lundquist et al., 2000), before reacquiring connection. These data outages prevent any systematic study of the nocturnal low-level jet as revealed by the rawinsonde soundings. Whiteman et al. (1997) also evaluated the first-reported wind measurement above the surface for the special rawinsonde ascents for two years at the Cloud and Radiation Testbed (CART) site in north-central Oklahoma, where the

TABLE I  
Performance characteristics for HRDL during CASES-99.

Wavelength ( $\mu\text{m}$ )	2.02
Range resolution (m)	30
Pulse repetition frequency (Hz)	200
Beam rate (Hz)	$\leq 8$
Minimum range (m)	250
Maximum range (km)	2–6
Velocity accuracy ( $\text{m s}^{-1}$ )	0.1
Maximum scan rate ( $^{\circ} \text{s}^{-1}$ )	60

sondes were tracked by LORAN. They found that the first wind value was below 100 m 83% of the time, with the majority of first reports at 50–70 m. Because at least a couple of points below  $Z_X$  are needed to define a jet, it is likely that some LLJs important to our study would be missed even by these carefully controlled rawinsonde data. Thus, for applications such as ours, where LLJ maxima below 100 m AGL are of interest, one must use caution in interpreting LLJ climatologies based on profiler or rawinsonde datasets.

## 2.1. HIGH-RESOLUTION DOPPLER LIDAR

HRDL is a scanning Doppler lidar system that maps out the Doppler-velocity field in the boundary layer with a range resolution of 30 m and a velocity precision of  $\lesssim 0.1 \text{ m s}^{-1}$ . Operating characteristics of HRDL are shown in Table I. A detailed technical description can be found in Grund et al. (2001) and Wulfmeyer et al. (2000), and the role of HRDL in CASES-99, in Blumen et al. (2001), Newsom and Banta (2002), and Poulos et al. (2002). In this study we use both azimuth and elevation scanning capabilities of HRDL.

We performed quality control procedures to reduce the effects of bad data on profiles derived from the Doppler velocities. A number of effects can degrade the Doppler signal quality. Two of the more significant are hard-target returns and occasional beams with poor signal quality. The first type occurs because the lidar beam sometimes intersects hard targets such as trees, towers, power lines, terrain, etc., when scanning at low elevation angles. Such hard-target returns, identified by large backscatter signal values *and* having Doppler velocities close to zero, are filtered out using these properties. For the second type of effect, weak signals produce high uncertainty in the Doppler frequency estimates, and therefore poor velocity estimates. These estimates are easily identified by small backscatter re-

turn signals, and are easily filtered out by rejecting backscatter values below an appropriate threshold level.

### 2.1.1. *Modified Velocity-Azimuth Display*

HRDL performs scans in azimuth and elevation. Azimuth scans at constant elevation through a full  $360^\circ$  trace out a cone in the atmosphere. Each conical scan took  $\sim 1$ – $2$  min to complete, and each individual scan can be used to calculate vertical profiles of the direction and speed of the horizontal wind, using the velocity-azimuth display (VAD) technique described by Browning and Wexler (1968). During CASES-99 these full conical scans were taken at irregular time intervals, so we developed a modified VAD technique that could provide wind profile data at regularly spaced time intervals. Unlike the conventional VAD method, which uses only the full  $360^\circ$  azimuth scans, the modified VAD approach makes use of data from each of the different scan types occurring in a given sampling interval, in this case 30 min. This new algorithm involves only a slight modification to the conventional VAD processing technique.

In this new method, all the Doppler radial velocity  $u_r$  data acquired during a given time period are divided into 10-m vertical bins, regardless of what kind of scan the data came from. A given bin may contain  $u_r$  measurements scattered over a variety of azimuth and elevation angles, depending on the scans performed during that period. It is assumed that within a vertical bin the mean wind is uniform and horizontal. The components of the mean wind  $U$  and  $V$  within a vertical bin are obtained by minimizing the total squared deviation between the radial component of the mean velocity, which is represented by a sine wave as in Browning and Wexler (1968), and the  $u_r$  measured by the lidar. This processing technique was applied to the entire HRDL CASES-99 data set using a 30-min averaging period oversampled at 15-min intervals.

The linear system that results from least squares minimization has no solution if all of the azimuth angles are the same during the averaging period. The system will be ill-conditioned if the difference between the minimum and maximum azimuth is small. Mean wind estimates derived from ill-conditioned linear systems as well as very noisy data are excluded based on quality parameters, which are proportional to the computed error in the retrieved mean velocity components. The quality parameters provide an objective method of rejecting bad estimates.

We determined the height  $Z_X$  of the maximum wind speed for each averaging period and noted the time, along with the speed  $U_X$  and the direction  $D_X$ , of this jet maximum. We also determined these quantities for vertical profiles from the individual conical scans using the conventional VAD technique.

### 2.1.2. *Vertical Cross Sections*

Sector scans in elevation produce vertical slices or cross sections of  $u_r$ . These scans took  $\sim 20$ – $35$  s to complete and were often performed repeatedly for an-

imation during the analysis. It was thus typical to have 50–100 such scans per hour, interspersed with VAD-type scans.

Vertical-slice scans were generally performed looking approximately along the mean wind vector, which was determined from the VAD-type scans. As a result, in situations where directional shear was small, profiles of the mean velocity component derived from vertical-slice scan data differ little from the mean wind-speed profiles obtained from either VAD algorithm described in the previous section. Profiles of the mean velocity component  $U(z)$  parallel to the scan plane and its variance  $\overline{u'^2(z)}$  were computed from vertical-slice scans as follows.

The horizontal wind component (parallel to the scan plane) was estimated from  $u_r$  measurements by dividing by the cosine of the elevation angle. This gives a good approximation to the horizontal component, provided the vertical velocity  $w$  component is much less than the horizontal component, or provided the scan elevations are small. Horizontal-velocity profiles derived from individual vertical-slice scans were obtained by sorting the data into 10-m vertical bins. Estimates of the mean and variance were obtained by averaging (horizontally) within each vertical bin. Variance estimates are more sensitive to measurement error than are the means, and this measurement error increases with distance from the lidar because of weakening return signal. Thus  $\overline{u'^2(z)}$  profiles sometimes do not extend as high as  $U$  profiles.

Each vertical-slice scan thus provides a vertical profile of  $U(z)$  and  $\overline{u'^2(z)}$ . At this point we can plot each profile on a time-height cross section of mean wind and wind-speed variance. This was done for each of the 12 nights when HRDL obtained good data. An example is given in Figure 3. Similar to the VAD procedure, we found the level of the jet maximum, then noted the time, the height  $Z_X$ , and the speed  $U_X$  for each vertical-slice scan (direction was not available from these scans). These data too were further averaged over 15-min intervals.

### 2.1.3. Analysis Methods

Our first method of viewing the  $U_X$ ,  $Z_X$ , and  $D_X$  time series was to plot data from each individual scan, including the standard VAD scans and each vertical-slice sweep. This procedure gave considerable confidence in the data and analysis, because (1) neighboring data points from each scan type showed strong consistency in time, and (2) data from the VAD profiles fell in line with the points from the repeated vertical-slice-scan profiles, even though the two methods represent very different ways of determining mean horizontal winds. An example of this consistency is given later in Section 4.2.

We then used the individual scan data to make histograms and scatter plots similar to those to be presented in Section 3. Because some nights and some time periods had more data than others, however, we were concerned that this might introduce a bias into the statistics. So we averaged the data from the vertical-slice profiles over 15-min and used the new VAD procedure, outlined in the previous section, which gave 30-min averages oversampled at 15-min intervals. This pro-

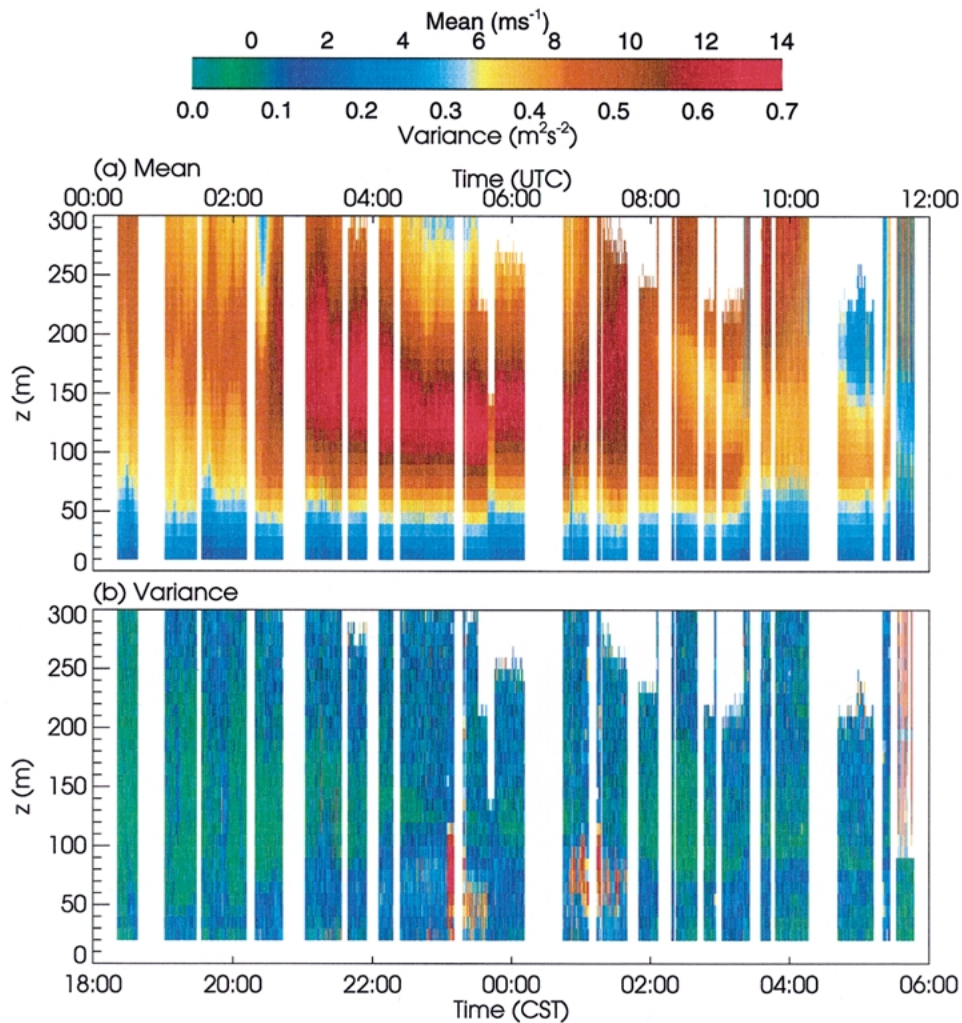


Figure 3. Sample time-height cross sections of mean wind speed (a) and variance of the radial wind component (b) calculated from HRDL vertical-slice scans. Each vertical line represents a vertical profile of the horizontally averaged wind speed or variance from the vertical cross sections, as described in the text. Gaps are where scans other than vertical-slice scans (such as conical scans) were performed, or where we changed tapes. The abscissa axis is hour of the night given both in CST (scale at (b)) and UTC (scale at (a)). Data are from 21 Oct 99 (Julian night 294) UTC.

cedure gave the same number of samples for each hour sampled. The resulting histograms and scatter plot presented in Section 3 differ little from those created from the individual-scan profiles. We also plotted the time series of  $U_X$ ,  $Z_X$ , and  $D_X$  using both individual-scan data from the conventional VAD algorithm and the 30-min averaged data from the new, modified VAD procedure, and again, the differences were minimal. The results presented in this study thus proved rather

insensitive to the use or method of further averaging of the profile data, which already represented a spatial average.

## 2.2. LLJ CRITERIA

Vertical profiles of the horizontal wind speed were determined using procedures described in the previous subsections. Examples of several types of profile that we found are shown in Figure 1. Some profiles showed the expected jetlike shape (e.g., Figures 1a,b) but others exhibited a flatter profile with height (Figures 1d–f). It is important to include these flat-profile jets in the LLJ sample, because they result from acceleration of the flow aloft after sunset by the Blackadar mechanism. Still other profiles had double maxima (Figure 1g) and even triple maxima (Figure 1h). The upper jet in Figure 1g was from a southwesterly direction and thus probably represents the Great Plains LLJ, whereas the lower jet represents the post sunset Blackadar acceleration down the near-surface pressure gradient.

The reason for the diversity of profile shapes is that sometimes the layer previously occupied by the daytime mixed layer accelerates more uniformly through its depth, and sometimes one level accelerates more strongly than the others. These differences are undoubtedly related to variations of the ageostrophic wind, or the geostrophic wind itself, with height (Mahrt, 1999). Another factor is that turbulence and mixing properties become vertically layered under stable conditions, and therefore also vary with  $z$ . Explaining the differences in the evolution of LLJ profile shapes is obviously an area where further work is needed.

We identified LLJs by visual inspection of each profile from each scan, but this was time consuming and would be impractical for larger datasets. Visual inspection was the preferred method for accuracy of interpretation, given the variable nature of the mean wind profiles as represented in Figure 1. However, to handle the large dataset quantitatively in a more efficient manner, we developed an objective, automated technique. The objective criteria we chose to define a LLJ were based on those of Andreas et al. (2000), which called for choosing those low-level wind-speed maxima that exhibited a decrease of at least  $2 \text{ m s}^{-1}$  at vertical levels both above and below the level of the peak value  $Z_X$ . Criteria used by Bonner (1968) and Whiteman (1997) caused us to exclude many jets that we felt obviously belonged in our sample, given the objectives of the study; for example, profiles resembling Figures 1c–h were rejected by using these criteria, but are of interest for this study.

Even using the Andreas criteria, we found as a result of the visual-inspection process that we were excluding an unacceptably large number of LLJs with the automated procedure. This turned out to be because many of the repeated vertical-slice scans were only scanned up to shallow elevation angles of  $10$  or  $15^\circ$ , and thus only reached heights of 200 to 250 m. Profiles similar to those in Figure 1e or f often were not high enough to show the needed decrease in wind speed aloft, and thus they were not classified as a LLJ. In these cases, deeper scans generally showed that this decrease did occur and the LLJs did represent an acceleration of

flow over daytime values in these layers, i.e., that they should have been classified as legitimate LLJs. Given the precision of HRDL and the fine vertical resolution in the calculated mean profiles, we felt justified in using smaller threshold criteria of 1.5, 1.0, and 0.5 m s<sup>-1</sup> to address this problem. We found that 0.5 m s<sup>-1</sup> gave the best agreement with visual determinations, and we used this value for the HRDL analysis. For the deeper scans that provided data higher in the SBL, we found little difference among the results based on any of the threshold criteria. However, because we also used sodar/profiler results, where we were not confident in using a difference of 1.0 m s<sup>-1</sup> or lower because of measurement uncertainty, we used a threshold of 1.5 m s<sup>-1</sup> for the sodar/profiler datasets.

### 2.3. PROFILER/MINI-SODAR COMBINATION

Boundary-layer radar-wind profilers (Eklund et al., 1988) provide wind profiles by transmitting a radar signal at 915 MHz and measuring the Doppler-shifted frequency of the backscatter from one vertical beam and two or four offset beams. Six minutes are required for one scan sequence; multiple scans were averaged together to create hourly averages of winds. These hourly averages are considered reliable to within  $\pm 1$  m s<sup>-1</sup>. The lowest level for which winds are available is typically  $\sim 150$  m, and range gates have a length of 60 m or more (in this study we used range gates of 60 m).

In the CASES-99 field program, three boundary-layer wind profilers were operated by the Argonne Boundary Layer Facility (Coulter et al., 1999). These profilers were collocated with sodars. Additionally, two boundary-layer profilers were operated by the National Center for Atmospheric Research (NCAR), but these sites collected no wind data below the lowest profiler range gate, so they are not included in this study.

The profiler-data quality control involved a two-step process: The first removed significant outliers in the consensus-averaged data by comparison with neighboring values, either in time or height; the second compared the variance of wind components within a given time-height domain and removed values that differed from the mean by more than 2 standard deviations in an iterative process. This second procedure was in place to remove 60-Hz noise effects. A bird-removal algorithm also operated on the profiler data during initial data collection; however, bird migration is from north to south at this time of year and generally did not pose a significant problem to this investigation, where wind directions were primarily from a southerly direction.

Three Doppler minisodars, collocated with the ANL boundary-layer profilers, were deployed both to provide a high-resolution wind profile between 10 m AGL and the lowest level of the boundary-layer profilers and as an independent confirmation of the winds at the lowest levels of the profilers (Coulter and Kallistratova, 1999). Sodars rely on the transmission of sound, and thus the sodar signal is directly dependent on the temperature and wind structure of the atmosphere. The

sodars have a 5-m range gate and are designed to collect data between 10 and up to 200 m; 15-min averages of these data are provided by ANL. For this study, these 15-min averages were further averaged into hourly profiles for better compatibility with the profiler data.

### 3. LLJ Frequency Distributions: Speed, Height, Direction

For many applications, and for assessing the representativeness of the CASES-99 dataset, the frequency of occurrence of speed  $U_X$ , height  $Z_X$ , and of the direction of the LLJ ( $D_X$ ), are important. We used the 15-min HRDL data and 1-h sodar/profiler data to generate histograms of these quantities. The two datasets are described separately to assess the similarities and differences due to the different instrumentation.

Histograms based on HRDL 15-min means of  $U_X$ ,  $Z_X$ , and  $D_X$  are shown in Figure 4. Most of the speeds of the jet maxima fell between 7 and 10 m s<sup>-1</sup>, with a mode of nearly 19% of the occurrences at 8–9 m s<sup>-1</sup>. The fact that the height of the LLJ's fell mainly around 100 m means that our  $Z_X$ 's are lower than in most other studies in the U.S. Great Plains. In the most recent study, for example, Whiteman (1997) found peaks in occurrence during both warm and cold seasons at 300–400 m AGL. To a large degree these differences reflect differences in study objectives and therefore in the definition of LLJ, but some of the differences are also instrumental: HRDL is ideally suited to detect  $Z_X$  in the 30–150-m range, whereas data from other instrumentation are often unavailable or unreliable at these altitudes, as described previously. It is also possible that October – or this particular October – had unusually weak winds and low LLJs.  $D_X$  was distributed over all quadrants, but showed a strong peak for southerly jets.

As an extension of the histogram analysis, we also plotted cumulative frequency distributions (Figure 5) and a plot of  $Z_X$  vs.  $U_X$  (Figure 6). The cumulative distributions show, e.g., that 46% of the jet maxima occurred below 100 m and 69%, below 140 m. The  $Z_X$  vs.  $U_X$  plots show a modest tendency for the stronger LLJs to occur at higher levels than the weaker ones, for this data set. One of the more interesting aspects of this plot is the absence of points in the lower right, indicating that the stronger jet maxima did not occur at low levels.

Histograms from the sodar/profiler data are given for each of the three sites (Figures 7–9). Jet speeds were broadly consistent with the 7–10 m s<sup>-1</sup> concentration in the HRDL data, but WHI showed a peak at lower wind speeds (4–6 m s<sup>-1</sup>), and BEA showed significant occurrences of stronger  $U_X$  of 14–20 m s<sup>-1</sup>.  $Z_X$  at BEA was similar to the HRDL data near Leon, with a peak at ~ 80–100 m AGL. Both WHI and OXF had peak occurrences somewhat higher at 120–140 m AGL. A major difference in the sodar/profiler  $Z_X$  data is the indication of more occurrences of maxima above 200 m, which would have been measured by the profiler. Profiler data, indicated by shading in the three figures, appear quantized in the histograms,

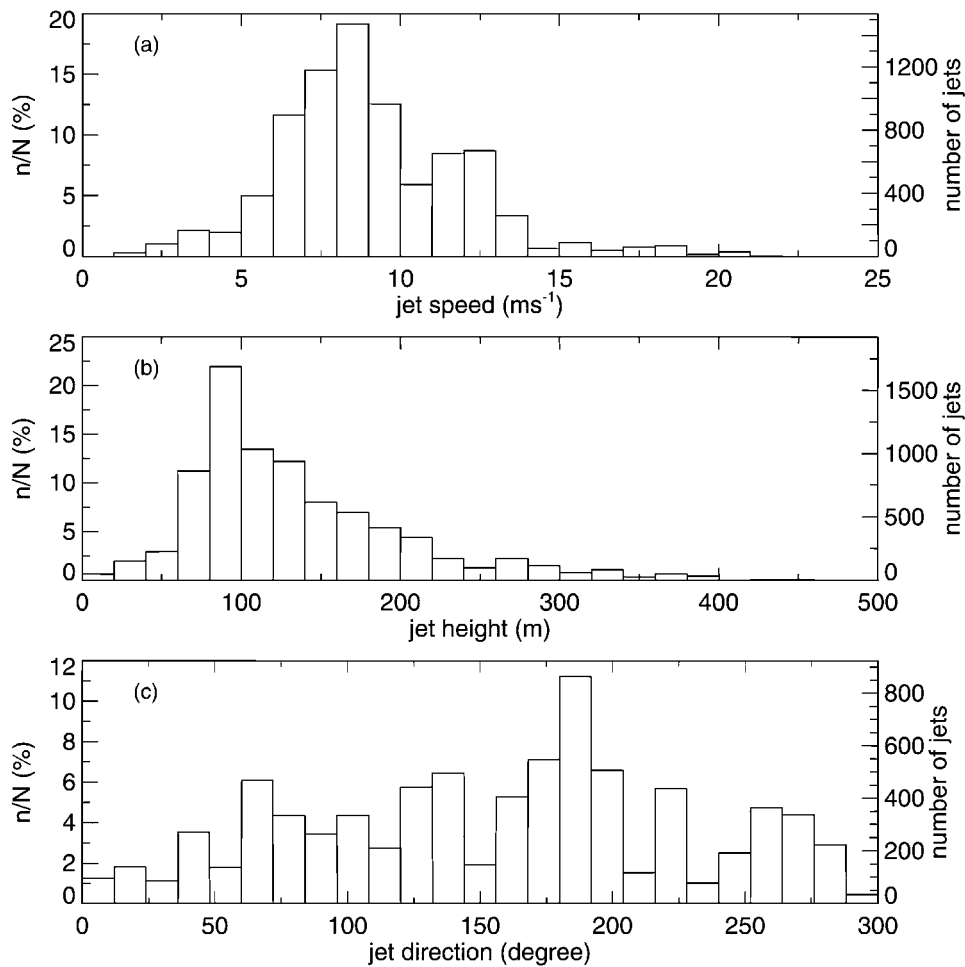


Figure 4. Histograms of jet speed  $U_X$  (a), height  $Z_X$  of maximum speed (b), and direction of jet maximum  $D_X$  (c). Data were compiled from means at 15-min intervals of each quantity, determined from HRDL vertical-slice and VAD-type scans as described in the text. Percentages of occurrences in each bin are shown along left vertical axis, and total number of occurrences in each bin is indicated along the right vertical axis.

because of the 60-m range-gate spacing. The peak in LLJ direction at all three profiler sites was southerly, in agreement with the HRDL data.

The histograms in Figures 7–9 indicate variations in  $U_X$ ,  $D_X$ , and  $Z_X$  between the three sites. To determine whether these variations reflected actual differences among the sites (as opposed to unequal sampling among profilers), we examined a set of 102 hourly nocturnal profiles where all three sites showed a jet profile using the Andreas  $1.5 \text{ m s}^{-1}$  criterion. The variations among the sites were calculated as an hourly spread: For each of the 102 hourly profiles, the spread was calculated as the difference between the maximum and minimum of the three values. We also

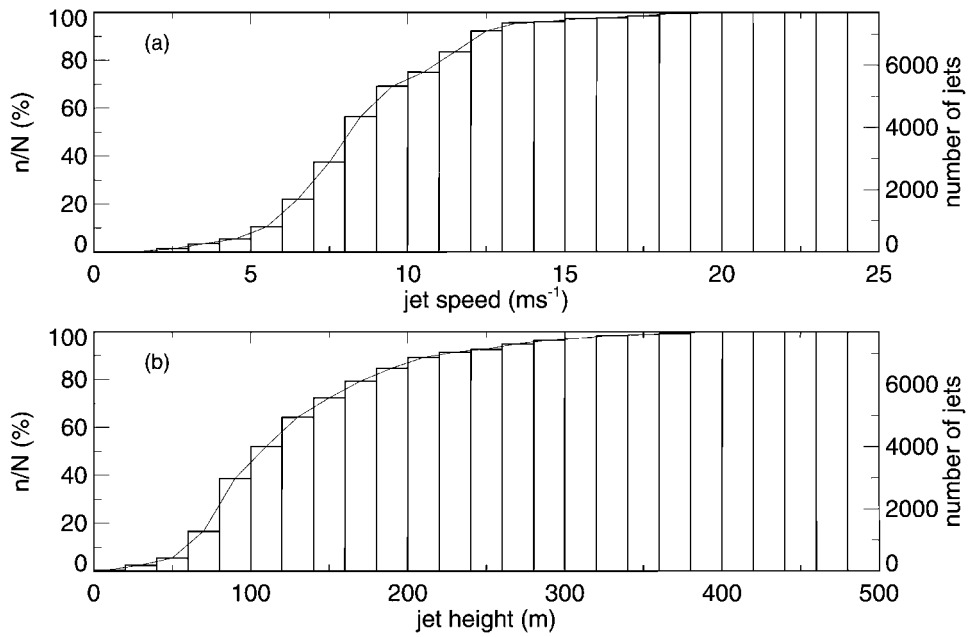


Figure 5. Cumulative distributions of  $U_X$  (a) and  $Z_X$  (b) based on data from Figure 4. Vertical axes are as in Figure 4, except for cumulative-distribution statistics.

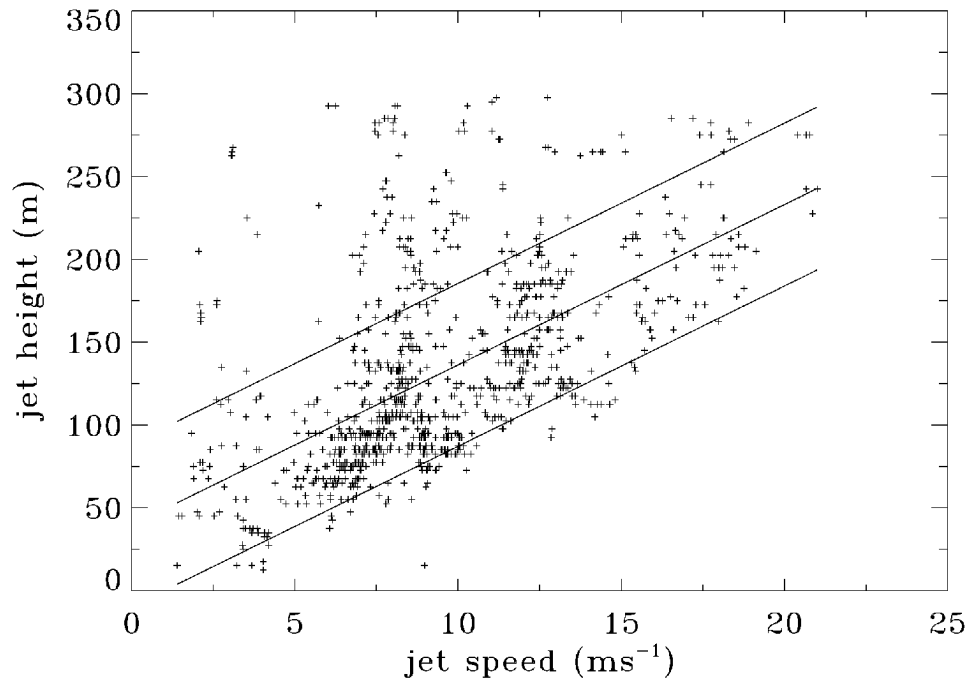


Figure 6. Scatter diagrams of  $Z_X$  vs.  $U_X$  from the same data as in Figure 4, taking only those values where  $Z_X < 300$  m. Middle line represents best-fit linear regression ( $R = 0.50$ ) and upper and lower lines are for  $\pm 1$  standard deviation.

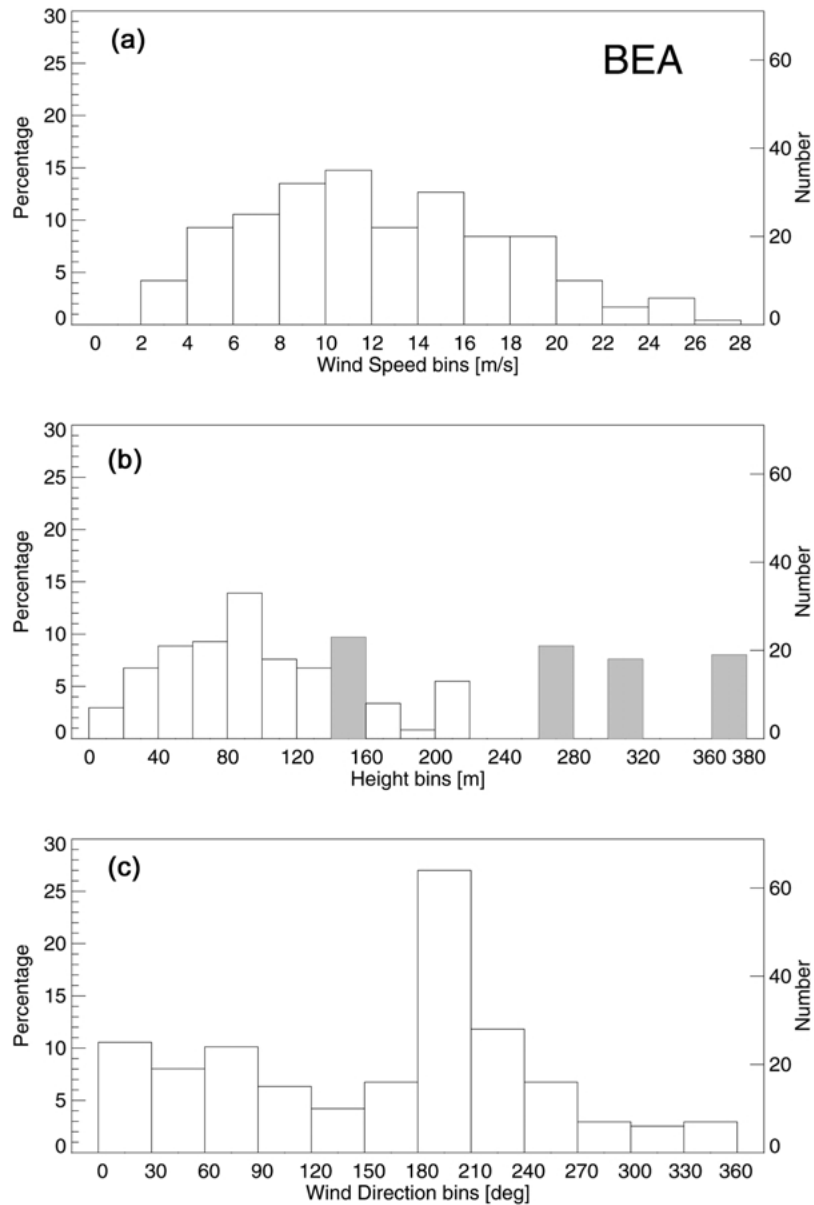


Figure 7. Distributions of the characteristics of LLJs identified in data from the Beaumont (BEA) sodar/profiler for the nighttime hours from 0000–1200 UTC, 3–31 October. (a) Depicts the distribution of wind speeds  $U_X$  at jet maximum. (b) Illustrates the distribution of the height levels at which the jet was observed  $Z_X$ . (c) Shows the distribution of wind directions  $D_X$  at jet maximum (0 degrees is from the north). Shaded bars indicate the levels of the profiler range gates, which are 60 m deep and lead to quantization of jet heights. For example, the bar at 260–280 m is based on the profiler range gate at 260 m and thus represents heights from 230–290 m. Bar at 140–160 m includes both the lowest profiler range gate at 145 m and sodar data. Plots represent 237 hourly samples.

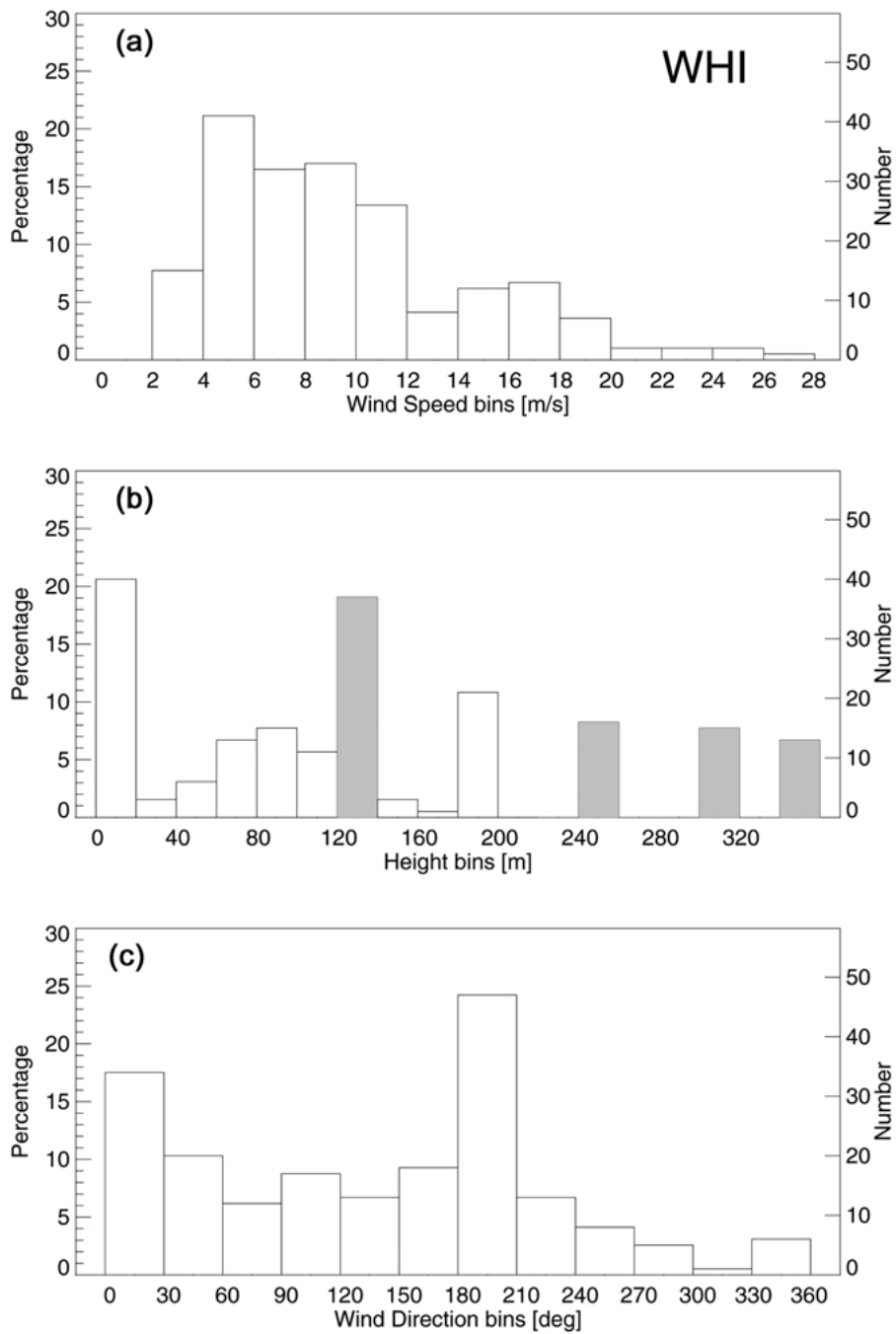


Figure 8. As in Figure 7, but of data from the Whitewater (WHI) site. The lowest profiler range gate at Whitewater was at 137 m AGL. Plots represent 194 hourly samples.

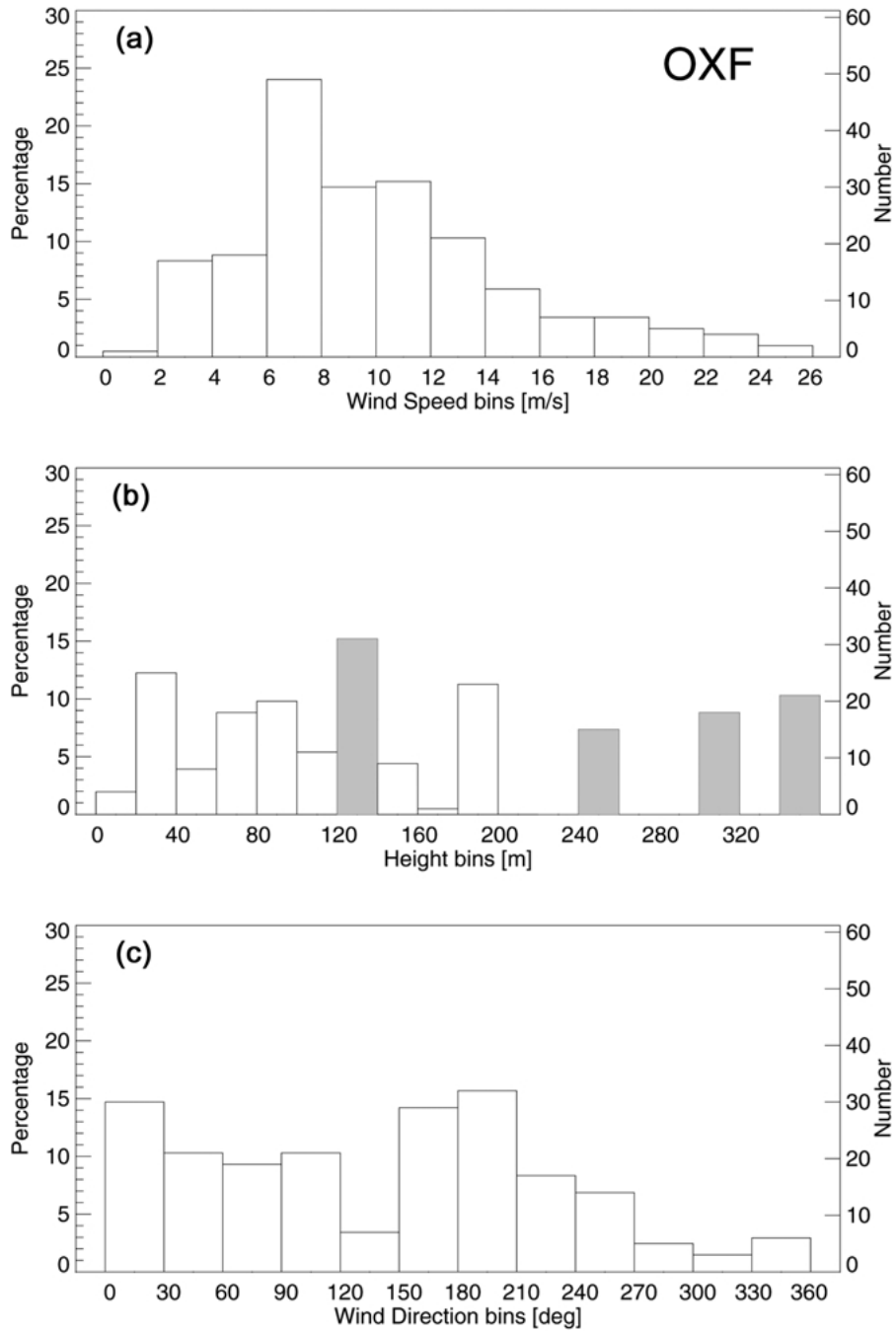


Figure 9. As in Figure 7, but of data from the Oxford (OXF) site. The lowest profiler range gate at Oxford was at 137 m AGL. Plots represent 204 hourly samples.

examined a subset of five nights with the best percentage of data returned (9, 11, 14, 21 and 24 October).

We found a small variation in  $U_X$  and  $D_X$  across the watershed. For the large set, the average spread in the wind speed was  $2.9 \text{ m s}^{-1}$ , with a standard deviation of  $2.5 \text{ m s}^{-1}$ . As the profiler accuracy is on the order of  $1 \text{ m s}^{-1}$ , we find this to be relatively good agreement, noting that this is probably an indication of the magnitude of the spatial variability of the wind speed over the spatial scale of the ABLE/CASES array. The subset of five nights shows similar agreement, with a mean spread of  $2.9 \text{ m s}^{-1}$  and a standard deviation of  $1.9 \text{ m s}^{-1}$ . The Beaumont site (BEA) had a slight preference for stronger jets: 40.2% of the profiles showed the strongest jet at BEA, whereas WHI showed the strongest jet in 30.4% of the 102 profiles, and OXF showed the maximum jet  $U_X$  29.4% of the time. The preference for strong jets at BEA is enhanced in the five-night subset: The strongest jets are at BEA in 53%, WHI in 21%, and OXF in 26% of the profiles.

The variability in jet wind direction across the watershed was similarly small. For the entire nocturnal CASES-99 dataset, the average spread in  $D_X$  was 6.5 degrees; for the subset of 5 nights, the average spread in wind direction was 7.2 degrees. Because a typical wind profile shows much larger variations in wind direction over the lowest 200 m, we find this agreement between stations to be excellent.

A discussion of the variation in jet height over the watershed is more problematic due to the nature of sodar and profiler data. If a jet were located above the top of the sodar data (200 m at best sodar performance but more often near 100 or 120 m),  $Z_X$  would be measured by the profilers, and the difference between the station elevations is on the order of the range gates of the profilers (60 m). Additionally, errors in estimating the jet height may be introduced when the jet maximum falls in a data-sparse region of the profile, where vertical resolution is coarse. Given these caveats, the data indicate that the LLJ height did not generally follow the local terrain slope, because the measured differences between  $Z_X$  on individual nights was usually significant. The station with the highest elevation, BEA, tended to have the lowest  $Z_X$  – for 62% of the time on all nights, and for 65% of the time on the five selected nights. The lowest site, OXF, exhibited the highest  $Z_X$  for 43.1% of the hourly intercomparisons for all nights and 39.5% of the profiles on the selected nights. This suggests that the height of the LLJ could be level (i.e., at a constant height MSL). Two specific examples where the jet was well defined at all three sites are shown in Figure 10. In the first case (14 Oct 0400 UTC/2200 CST) the jet was level, and in the second (11 Oct 0700 UTC/0100 CST) it followed the topography. The night of the first example, 14 Oct, was interesting, because  $Z_X$  at all three sites started out at the same height AGL (i.e., terrain following) for several hours after sunset, and then became level (at same height MSL) later in the night. The sodar/profiler data for all nights are being studied in greater detail for these effects. Further information on the relative  $Z_X$ 's at each of the sites is given in the time series plots in the next section.

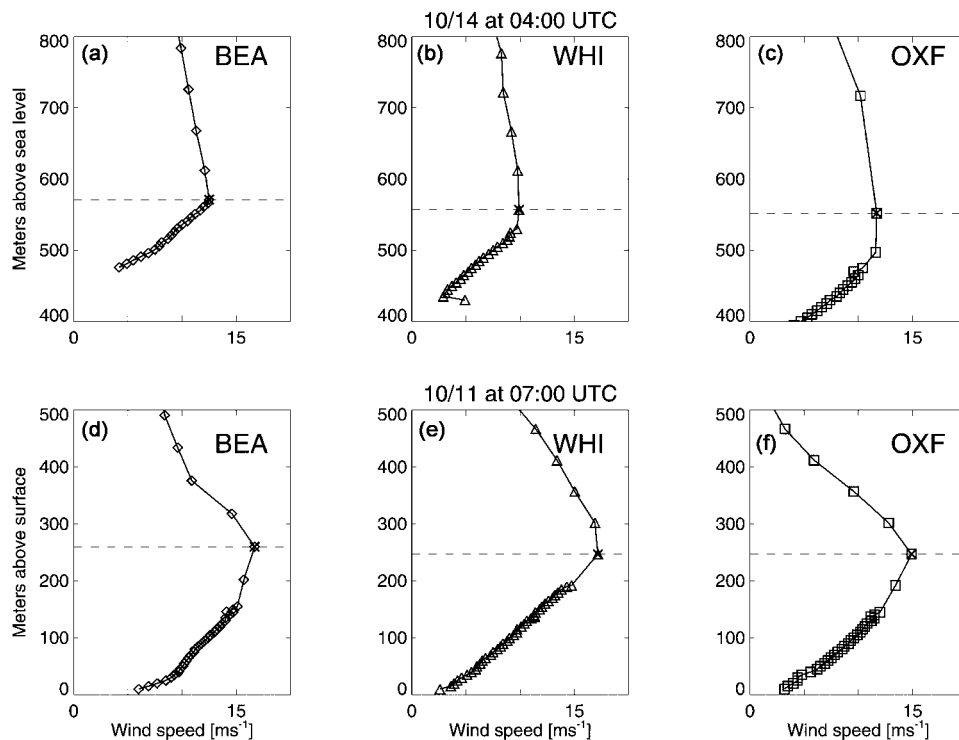


Figure 10. Regional variability of the low-level jet as seen in profiler/sodar data. (a–c) Show wind speed profiles from 0400 UTC 14 October at Beaumont, Whitewater, and Oxford, where altitude has been adjusted for station elevation. Dotted line marks the level of the LLJ as determined with the Andreas criterion with a wind speed difference of  $1.5 \text{ m s}^{-1}$ . All three sites show the jet at approximately 570 m MSL, indicating the jet height on this night was independent of terrain and therefore approximately level. (d–f) Depict wind speed profiles from 0700 UTC 11 Oct; the altitude is AGL and has not been adjusted for station elevation. LLJ at this time follows terrain quite closely, and is located at 250 m above the surface at all three sites.

These October 1999 findings can be put into the context of the total CASES dataset of warm-season measurements. Inspection of three years of data (April through September) from the ABL data archives indicate that the height of the jet above the Walnut River watershed lies, in the mean, between geopotential (level) and constant height above the surface (terrain following). Speed and height of the jet are often larger and lower, respectively at the highest (Beaumont) site. Although no systematic study of LLJ characteristics for the entire multi-year, warm-season ABL data set has been performed to date, inspection of the data suggests that the large number of cases with speeds less than  $10 \text{ m s}^{-1}$  and heights less than 100 m seen during CASES-99 is not necessarily characteristic of the 3-year data set. We anticipate that a careful study of these LLJ properties, with an appropriate LLJ definition and attention to quality control at and below 100 m AGL, will be done

at some point, perhaps after the conclusion of the ABLE project, when the data set is complete.

#### 4. Nighttime LLJ Evolution

Temporal behaviour of LLJ characteristics have been hypothesized to be related to the appearance of turbulence and vertical mixing processes in the SBL near the surface, e.g., acceleration of the LLJ leads to increased shear and increased turbulence near the surface. To investigate these relationships, it is thus critical to know how the LLJ evolves through the night. In this section we present time series of  $U_X$ ,  $Z_X$ , and  $D_X$  through the night. The time series represent the *nighttime* behaviour; the evening and morning transitions will be addressed in future studies. Analyses presented here were averaged over 15-min periods for HRDL and 1-h periods for sodar/profiler data. They begin at 0000 UTC (1800 CST), by which time the LLJ has at least begun to form, and on some evenings was fully formed, and they end at 1400 UTC (0800 CST).

##### 4.1. TIME SERIES OF $U_X$ , $Z_X$ , AND $D_X$

For presentation we divided the nights into four categories: high wind (15–20  $\text{m s}^{-1}$ ), high moderate wind (10–15  $\text{m s}^{-1}$ ), low moderate wind (5–10  $\text{m s}^{-1}$ ), and low wind (0–5  $\text{m s}^{-1}$ ) plus miscellaneous cases. Although these divisions are arbitrary, similarities within and differences between groups suggest that they may be functional for this particular data set. A Richardson number or similar characterization would be more appropriate, and a goal of future, more detailed case studies will be to determine more appropriate parameters to characterize LLJ behaviour. The four categories and the nights that fell into each category are given in Table II.

##### 4.1.1. High Wind-Speed Jets (15–20 $\text{m s}^{-1}$ )

Nights when  $U_X$  was greater than 15  $\text{m s}^{-1}$  for at least 4 h (Figure 11) also exhibited high turbulence levels for nearly all of the nighttime period after 0300 UTC (2100 CST). This was determined from plots (not shown) similar to Figure 3, which indicated that values of  $\overline{u^2(z)}$  exceeding 0.4  $\text{m}^2 \text{s}^{-2}$  extended from just below  $Z_X$  down to the surface. On 25 and 27 October,  $U_X$  increased steadily through the night from 10  $\text{m s}^{-1}$  at 0200–0300 UTC (2000–2100 CST) to 20  $\text{m s}^{-1}$  by 1100 UTC (0500 CST). Only a few hours of HRDL data were recorded on 28 October, but profiler data indicated 20  $\text{m s}^{-1}$   $U_X$  values until 0800 UTC (0200 CST). The jet height  $Z_X$  was variable in time at the HRDL site and also at the other sites as indicated by the profiler data.  $Z_X$  tended to be above 100 m except at BEA (which was consistently lower than the other sites on 25 and 27 October), as the high wind speeds seemed mostly incompatible with very low jet heights, as noted in the discussion of Figure 6. The direction tended to be steady, with slight veering through the night.

TABLE II

UTC night	Local night (October)	Julian night (UTC)	IOP	Mean LLJ speed ( $\text{m s}^{-1}$ )
<i>High wind nights</i>				(VAD)
25 Oct	24–25	298	–	15.2
27 Oct	26–27	300	12	14.6
28 Oct	27–28	301	–	13.2
<i>High-moderate wind nights</i>				
14 Oct	13–14	287	6	10.8
21 Oct	20–21	294	9	10.6
23 Oct	22–23	296	10	12.5
<i>Low-moderate wind nights</i>				
6 Oct	5–6	279	2	9.3
10 Oct	9–10	283	3	8.2
18 Oct	17–18	291	7	6.8
24 Oct	23–24	297	–	7.6
<i>Light wind, misc. nights</i>				
26 Oct	25–26	299	–	3.8
20 Oct	19–20	293	8	7.6
5 Oct	4–5	278	1	8.2

#### 4.1.2. High Moderate Winds ( $10\text{--}15 \text{ m s}^{-1}$ )

On nights with high-moderate winds of  $> 10 \text{ m s}^{-1}$  for at least several hours (Figure 12),  $U_X$  increased early in the evening until 0400 UTC (2200 CST). This occurred gradually on 14 and 23 October, but very suddenly ( $< \frac{1}{2}$  h) on 21 October.  $Z_X$  was generally above 100 m and again variable in time, and on 14 and 21 October, BEA tended to have the lowest  $Z_X$ . After 0700 UTC (0100 CST) on 21 October discrepancies in HRDL-measured jet heights were partly due to the development of a double jet structure, with one jet at  $\sim 150$  m and another just below 300 m (see Figure 1g). We hypothesized in Section 2.2 that this is an example of LLJs at two different levels, responding to two different scales of horizontal pressure gradient—the lower jet to a more local scale, and the upper one to the Great-Plains – scale forcing. High  $\overline{u_r'^2(z)}$  turbulence bursts below jet level occurred at times, but not as continuously as in the previous case.  $D_X$  veered strongly through the night on 14 October from NE to SE, and data from the other nights showed slight veering.

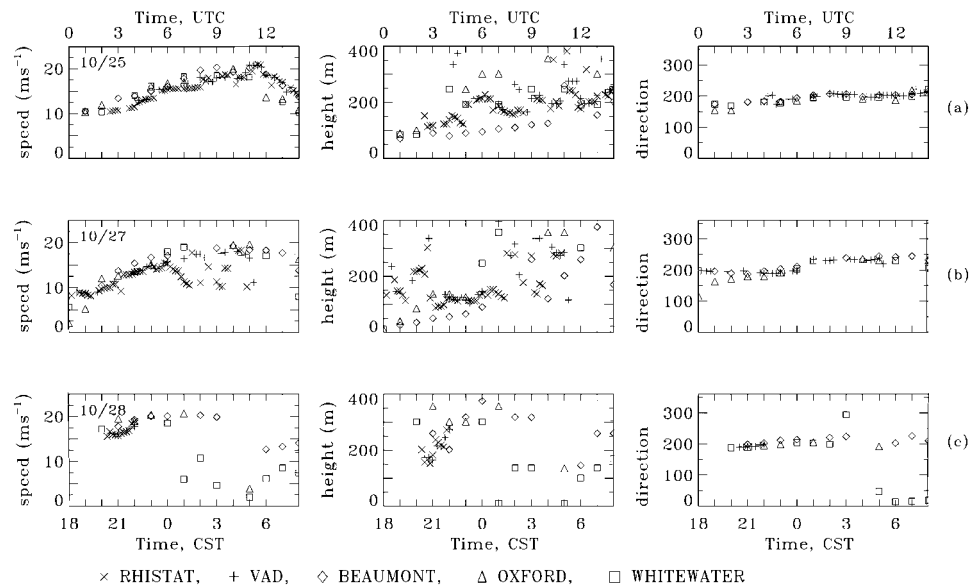


Figure 11. Time-series plots of LLJ characteristics for high jet-speed ( $> 15 \text{ m s}^{-1}$ ) nights: (a) Top row, 25 October; (b) middle row, 27 October; and (c) bottom row, 28 October (all dates are UTC). Abscissa is time of night in hour UTC (top) and hour CST (bottom). Ordinate of first (left) column is maximum jet speed  $U_X$  ( $\text{m s}^{-1}$ ), second (middle) column is height  $Z_X$  of maximum speed, and third (right) column is wind direction at the level of maximum speed  $D_X$ . Symbols are as follows:  $\times$ , determined from HRDL vertical-slice scans,  $+$ , determined from HRDL VAD-type scans, and open symbols represent sodar/profiler data from  $\diamond$  Beaumont (BEA),  $\square$  Whitewater (WHI), and  $\triangle$  Oxford (OXF).

#### 4.1.3. Low Moderate Winds ( $5\text{--}10 \text{ m s}^{-1}$ )

On two of the four low moderate wind nights (Figure 13),  $U_X$  increased early in the evening, but on the other two nights (18 and 24 October), the peak speeds were remarkably steady all night from the start at 0000 UTC (1800 CST).  $Z_X$  was again much more variable both in time (as measured by HRDL) and in space than  $U_X$ . It tended to be at or just below 100 m, with upward excursions confined to under 200 m after 0200 UTC (2000 CST), i.e., no really high jets. Three of the four nights showed significant veering through the night. Although 24 October showed bursts of  $\overline{u'^2(z)}$  exceeding  $0.3 \text{ m}^2 \text{ s}^{-2}$  between the surface and  $Z_X$  after midnight (0600 UTC), turbulence levels overall were relatively low on these nights. An exception was a period of less than  $\frac{1}{2}$  h on 6 October around 0530 UTC (2330 CST), when shear-instability waves generated significant mixing just below  $Z_X$ , as reported by Newsom and Banta (2002) and Blumen et al. (2001). Another interesting night was 18 October, when three density-current or solitary-wave events were evident in the temperature and other records (Sun et al., 2002).

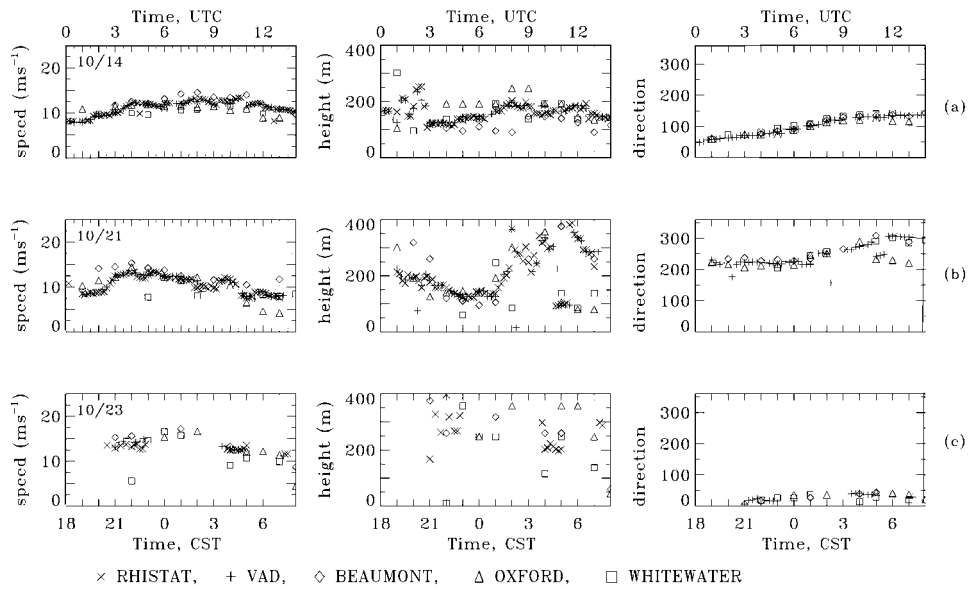


Figure 12. Time series plots of LLJ characteristics for high-moderate jet speed nights, as in Figure 11. (a) Top row, 14 October; (b) middle row, 21 October; and (c) bottom row, 23 October.

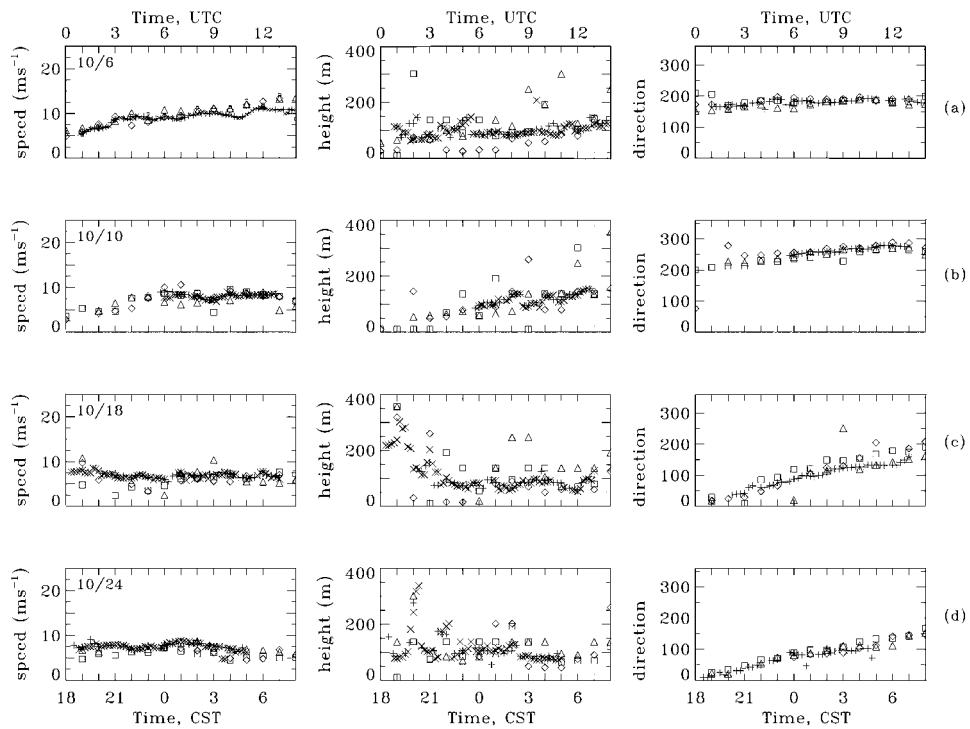


Figure 13. Time series plots of LLJ characteristics for low-moderate jet speed nights, as in Figure 11. (a) Top row, 6 October; (b) second row, 10 October; (c) third row, 18 October, and (d) fourth (bottom) row, 24 October.

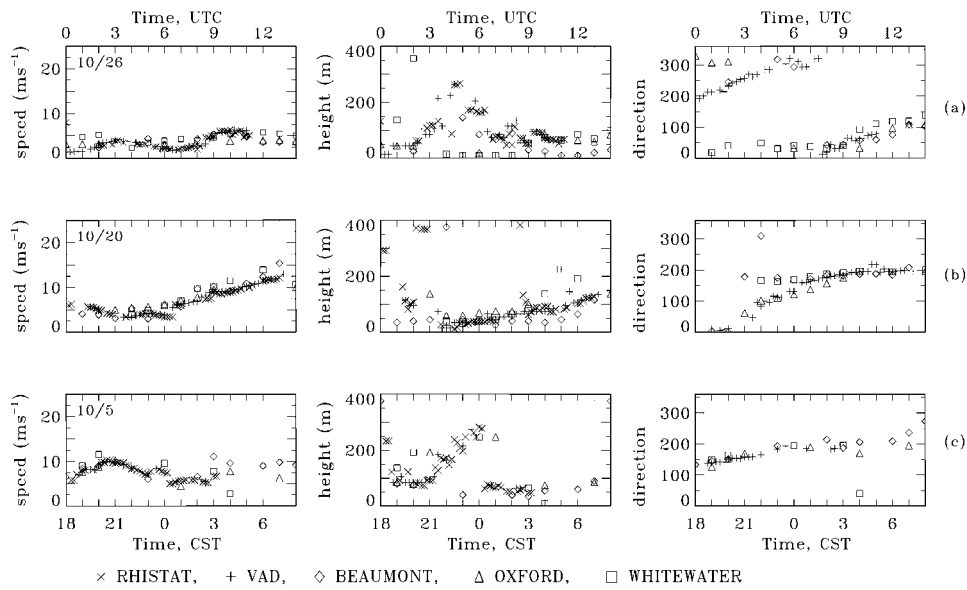


Figure 14. Time series plots of LLJ characteristics for low wind speed night and miscellaneous nights, as in Figure 11. (a) Top row, 26 October; (b) middle row, 20 October; and (c) bottom row, 5 October.

#### 4.1.4. Low Wind Speeds ( $< 5 \text{ m s}^{-1}$ ) and Miscellaneous Cases

The only low wind-speed case (Figure 14) occurred on 26 October. This light-wind, low-level maximum was evident at all sites.  $Z_X$  was often difficult to determine and varied in time and space. After 0730 UTC (0130 CST) an easterly surge, apparently related to drainage from the Flint Hills near BEA (see Figure 2) produced an increase in  $U_X$  at the HRDL site.

The night of 20 October was unusual, because it began with a low, weak jet, but by midnight (0600 UTC) the speeds began to increase dramatically from a southerly direction. On 5 October, the first night of intensive operations,  $U_X$  and  $Z_X$  appeared more variable than on other nights, and thus made it difficult to classify.

## 4.2. SMALLER-SCALE BEHAVIOUR

The time series findings in the previous section were based on averaged quantities at 15-min intervals derived from HRDL data. Analyses based on individual scan data also showed interesting behaviour at finer temporal resolution. For example, Figure 15a shows quasi-periodic fluctuations in the speed and height of the LLJ as the jet speed increased early in the evening of 14 October. The period of these fluctuations was somewhat less than 10 min, and they may be associated with pressure fluctuations sensed at the surface (Cuxart et al., 2002). Figure 15b shows that these kinds of fluctuations were also present early on 21 October, indicating that they may be part of the evening transition process. Figure 15b also shows that the rapid increase in  $U_X$  noted in Figure 12 actually took place between 0225 and 0245 UTC

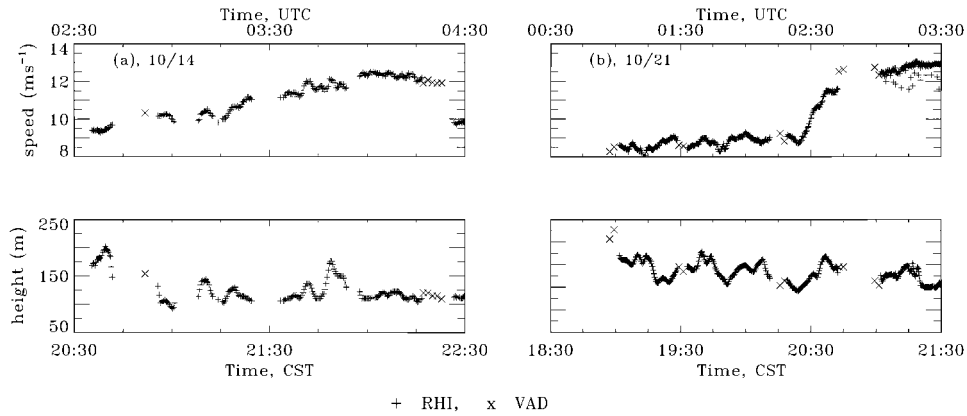


Figure 15. Time series of  $U_X$  (top) and  $Z_X$  (bottom) determined from individual HRDL vertical-slice (+) and VAD ( $\times$ ) scans, as opposed to averaged over a time interval as in the previous 4 plots. (a) 0230–0430 UTC on 14 October, and (b) 0030–0330 UTC on 21 October.

(2025 and 2045 CST), i.e., over a span of 20 min. The scan to-scan consistency in the trends of these quantities and the consistency between the vertical-slice scan data and the VAD-determined data provide confidence that these fluctuations are real atmospheric phenomena.

## 5. LLJ-Turbulence Interactions

To illustrate the relationship between LLJs and turbulence below the jet, we show data from two nights, a high-wind night (25 October) and a high-moderate wind night (21 October). Mahrt and Vickers (2002) suggested two criteria for detecting when turbulence is predominantly being generated at levels above the surface and transported downwards, the ‘upside-down boundary layer’: (1) Turbulence kinetic energy (TKE) increasing with height and (2) the vertical turbulent flux of TKE being directed downward (i.e., having negative values). TKE flux is  $\overline{w'(u'^2 + v'^2 + w'^2)}$  where in this case the overbar denotes a temporal average and the prime, a deviation from this average.

These quantities were calculated from the 60-m tower data after high-pass filtering the data at 20 s, and are presented as time-height cross sections (Figure 16). To compute TKE, we detrended each velocity component by high-pass filtering in the frequency domain, and performed an FFT of the 20-Hz data over a 6-hour period. The resulting spectrum was set to zero for  $|f| < f_{co}$ . In this case we chose the cut-on frequency  $f_{co}$  to eliminate fluctuations with periods longer than 20 s, so  $f_{co} = 1/20$  Hz. We then inverse-transformed this modified spectrum back into the time domain and computed TKE using a 40-s averaging period, oversampled at 20 s intervals.

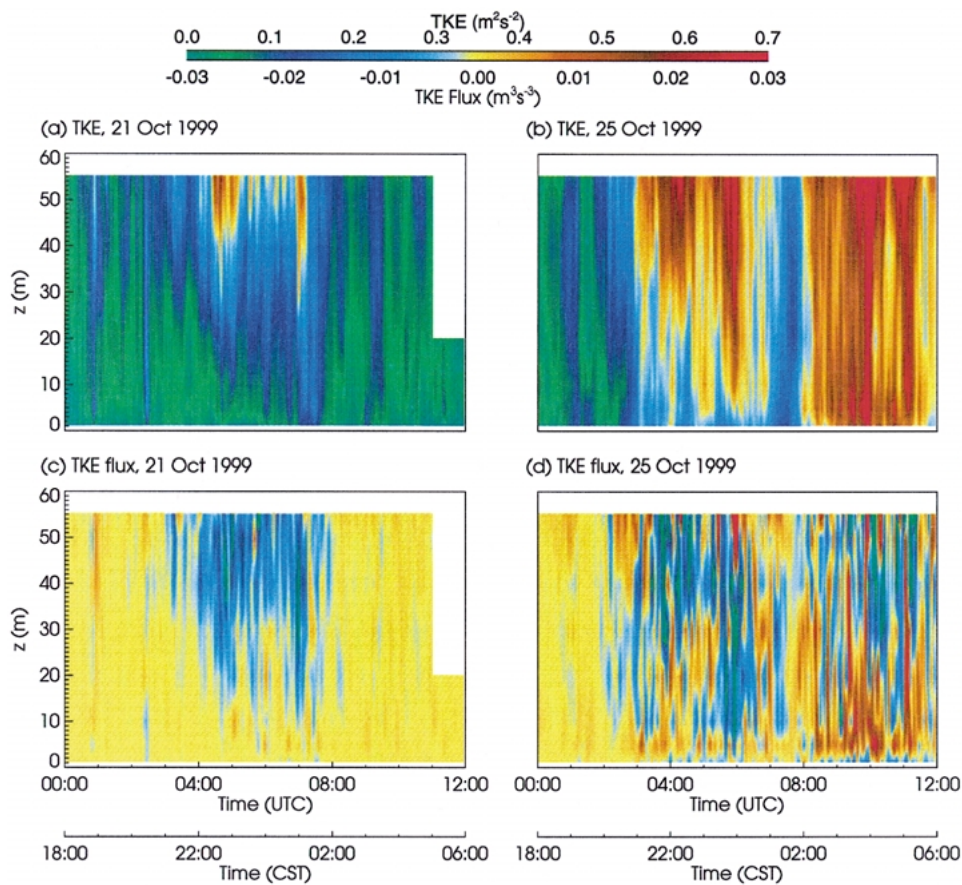


Figure 16. (a) TKE and (c) the vertical flux of TKE for the night of 20–21 October 1999. (b) TKE and (d) the vertical flux of TKE for the night of 24–25 October 1999. In (c) and (d) negative values imply downward mixing of TKE.

The cross sections for 21 October, a night when the LLJ was mostly  $10\text{--}13\text{ m s}^{-1}$ , show a period of high turbulence with two major peaks in the middle of the night between 0400 and 0800 UTC (2200 and 0200 CST), consistent with the HRDL data from the same night shown in Figure 3b. TKE clearly increased with  $z$  during this episode, and the vertical TKE flux, which had low values for most of the night, was strongly negative during the episode. Vertical profiles of these quantities at 0440 and 0700 UTC (2240 and 0100 CST; Figures 17a,b) show TKE increasing with  $z$  and negative TKE flux reaching a peak negative value near 30–40 m AGL, as found by Mahrt and Vickers (2002).

On 25 October, the high-wind night, high levels of TKE were evident most of the time after 0300 UTC (2100 CST). The pattern of relatively quiet turbulence levels before 2100 CST, followed by greater turbulence activity, was typical of many nights of CASES-99. The TKE pattern was complex: periods where TKE

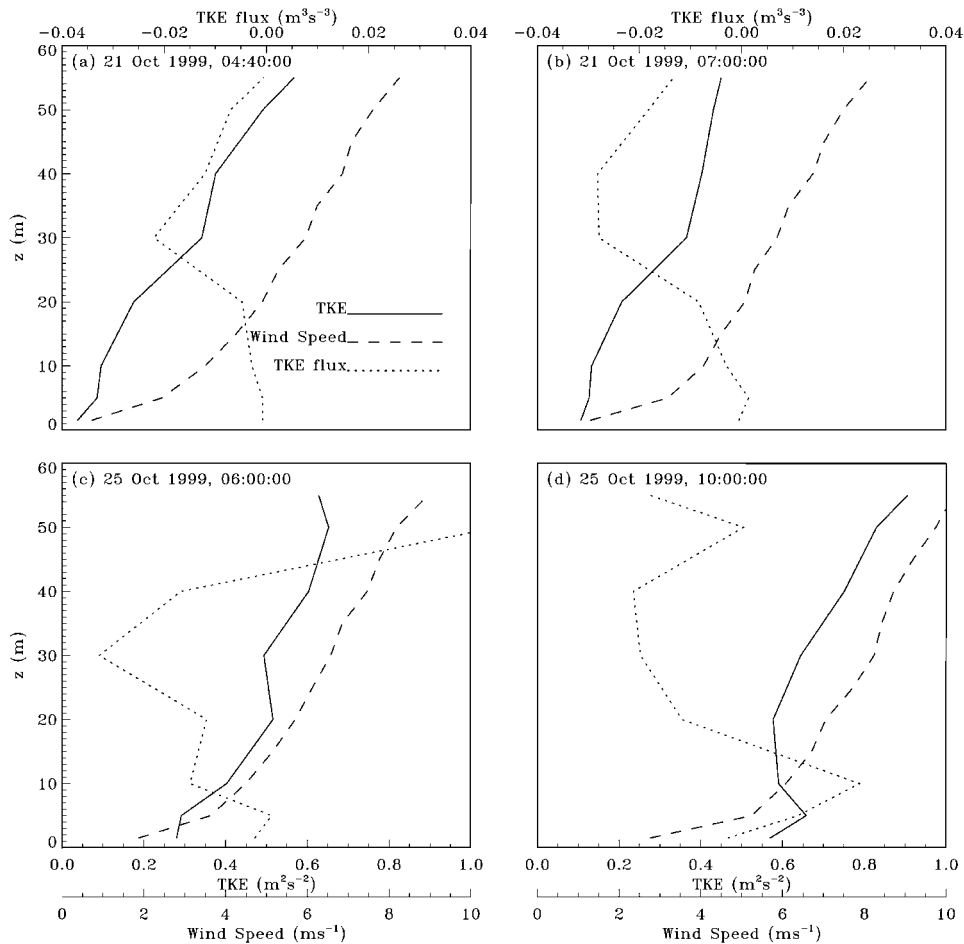


Figure 17. Representative profiles of TKE, TKE flux and mean wind speed for the night of 20–21 October 1999 (a) 20/2240 CST and (b) 21/0100 CST and the night of 24–25 October 1999 (c) 25/0000 CST and (d) 25/0400 CST. Mean wind speeds were computed at twelve levels on 60-m tower using 40 s averages of both sonic anemometer and prop-vane data. TKE and TKE flux were computed from only the sonic anemometer data (eight levels).

increased with height are evident, especially above 30 m AGL, and other periods where TKE appeared to decrease with  $z$ , especially after 0800 UTC (0200 CST) and below 30 m, are also apparent. The TKE vertical-flux pattern was even more complex, with intermittent periods of both positive and negative values. Sample profiles at midnight (0600 UTC; Figure 17c) illustrate the increasing TKE with  $z$  and the negative TKE flux, as seen in the profiles in the 21 Oct case. Later profiles at 1000 UTC (0400 CST) show decreases in TKE with  $z$  between  $\sim 5$  and 20 m associated with positive TKE flux there, indicative of turbulence generated near the surface. Above 20 m, however, the behaviour of TKE and TKE flux were the same as in the previous examples. Overall, we find numerous examples of turbulence

transported downward from jet level on nights with strong or moderately strong jets; in fact, this behaviour seems predominant during periods of strong turbulence (HRDL variance values  $> 0.3 \text{ m}^2 \text{ s}^{-2}$ ). We also found evidence of the more normal behaviour, when TKE decreased with height above the surface and TKE flux was positive. These occurrences, which indicate TKE being generated in the strong shear next to the surface and then exported upward, tended to be at lower levels, often below  $\sim 30 \text{ m}$ , in agreement with the results of Mahrt and Vickers (2002). Obviously, we will learn much about the interaction between LLJ behaviour and turbulent mixing below the jet by studying these and other cases individually in much greater detail.

## 6. Conclusions

This investigation of LLJ behaviour and effects has taken advantage of two unique aspects of the CASES-99 dataset in south-central Kansas: the vertical and temporal resolution of the HRDL scan data and the location and separation of three sodar/profiler sites. The fine resolution of the HRDL data has allowed us to focus on the first wind speed maximum above the surface produced by nocturnal decoupling of the flow. This maximum is most likely responsible for the production of shear and the generation of turbulence between the surface and the LLJ, and understanding its behaviour is believed critical to further understand nighttime mixing processes between the atmosphere and the surface. The combination has allowed us to determine the overall typical characteristics (height  $Z_X$ , speed  $U_X$ , and direction  $D_X$ ) of the LLJs seen during the October 1999 experiment, to investigate the spatial variability of LLJ properties across the 60-km watershed study area, to study the evolution of LLJ characteristics through many nights, and to look at the relationship between the LLJ and turbulence properties on two study nights.

The overall behaviour was characterized by the frequency of occurrence of several key LLJ properties. The mode in the  $U_X$  histogram at the main site was at  $8\text{--}9 \text{ m s}^{-1}$ , but this was site dependent: the highest site tended to have the fastest speeds and the lowest site, the slowest speeds. The high frequency of jets with  $Z_X$  near and below 100 m AGL is potentially significant for wind-energy applications. Comparisons among the data for the three sites at individual hours showed that the  $U_X$  and  $D_X$  tended to be similar across the region, but  $Z_X$  was more variable in space. The highest station (BEA) tended to have the lowest  $Z_X$ , indicating that in general the jet was not terrain following, but it could be close to level at least at times. These findings indicate that the structure of the LLJ was as a sheet or extensive layer of high-momentum flow over the entire region.

The time series of jet characteristics showed that, for the strongest wind cases ( $> 15 \text{ m s}^{-1}$ )  $U_X$  increased through the night, but for the other cases  $U_X$  tended to be relatively constant in time.  $Z_X$ , on the other hand, was much more variable for all wind-speed categories. This suggests that changes in the shear below the

jet could be due to changes in the height rather than the speed of the jet. High time resolution achieved by plotting data from individual HRDL scans showed that the speed and height sometimes fluctuated on time periods of several minutes. Whether these undulations have an effect on processes near the surface is under investigation. During several periods of high turbulence noted in the analysis of Doppler-lidar data, we found that these events were characterized by turbulence generated aloft and transported downward, in accordance with the so-called upside-down boundary-layer model.

If it were to be shown that turbulence generated in the shear layer below the jet does have a significant role in regulating surface fluxes, this would have important implications for NWP model results, especially for nighttime periods or multi-day simulations. Reasons for this are because, as mentioned previously, LLJs that may influence surface fluxes are not well represented in these models, and turbulence generated by LLJ shear is not included in model physics (Mahrt, 1998, 1999). Night occupies on average about half of the diurnal cycle. If surface-atmosphere exchange processes are poorly represented during this significant period (and can be shown to be of sufficient magnitude), then budgets of atmospheric quantities, including momentum, heat, and trace species, could be in error, with the error increasing in time as the length of the simulation includes more nighttime periods. This error would be a result of the fact that the surface often acts as a significant sink or source of these quantities, and the response of NWP models to stable conditions is to simply shut down the exchange processes to very low values. Neglect of such processes would be expected to jeopardize the accuracy not only of the budgets, but of numerical forecasts themselves as the number of days increases. Another significant problem is that numerical models are being extended to applications where the direction and magnitude of horizontal transport becomes important, such as air pollution and emergency response. Predictions involving these effects and extending over a nighttime or multi-day period would likely be unreliable.

To address such deficiencies, an overall objective of CASES-99 was to understand, and then to suggest ways to model and parameterize, turbulence and fluxes in the SBL. Characterization of the LLJ in space and time as in the present study is seen as one of several first steps. Important next steps include using individual case studies and case-study events (such as Blumen et al., 2001; Newsom and Banta, 2002; Sun et al., 2002; Mahrt and Vickers, 2002; Cuxart et al., 2002) to further probe the role and importance of turbulent fluxes, generated in the shear layer below the jet, in the vertical transport of quantities between the surface and the atmosphere, and to determine whether the magnitudes of these exchange processes are large enough to have an impact on the budgets. A further critical step is to understand the larger-scale and surface-boundary controls, i.e., what determines the behaviour of the LLJ on a given night.

### Acknowledgements

Funding for analysis and field measurements was provided by the Army Research Office under proposal #40065-EV and Grant DAAD19-9910249 [LM], and the Center for Geosciences/Atmospheric Research at Colorado State University. The National Science Foundation (Grants # ATM-9908453 [HRDL] and # ATM-9903645 [JKL]), the U.S. Department of Energy (DOE), Office of Science, Office of Biological and Environmental Research under contract W-31-109-Eng-38 [RLC], and the DOE National Renewable Energy Laboratory (IA No. DE-AI36-01GO11066) also provided funding for the field measurements and/or analysis. The authors are indebted to: J. Otten, Dr. W. Eberhard, and M. Pichugin for important contributions to HRDL data acquisition; Dr. V. Wulfmeyer, S. Sandberg, J. George, Dr. W. A. Brewer, A. Weickmann, R. Richter, and Dr. R. M. Hardesty for HRDL preparation and setup; Dr. J. Sun, S. Burns, Dr. S. Oncley, and N. Chamberlain for tower and sounding data; Dr. W. A. Brewer and B. McCarty for contributions to the analysis of the scan data; Dr. Christoph Senff and Dr. Jeff Hare for reviews of the manuscript; Dr. G. Poulos, Dr. W. Blumen, and Dr. D. Fritts for organizing the CASES-99 field project, J. Klazura for local arrangements, and J. Lucas and other ANL personnel for the profiler/sodar data.

### References

- Andreas, E. L., Claffey, K. J., and Makshtas, A. P.: 2000, 'Low-Level Atmospheric Jets and Inversions over the Western Weddell Sea', *Boundary-Layer Meteorol.* **97**, 459–486.
- Banta, R. M., Senff, C. J., White, A. B., Trainer, M., McNider, R. T., Valente, R. J., Mayor, S. D., Alvarez, R. J., Hardesty, R. M., Parish, D. D., and Fehsenfeld, F. C.: 1998, 'Daytime Buildup and Nighttime Transport of Urban Ozone in the Boundary Layer during a Stagnation Episode', *J. Geophys. Res.* **103**, 22,519–22,544.
- Blackadar, A. K.: 1957, 'Boundary Layer Wind Maxima and their Significance for the Growth of Nocturnal Inversions', *Bull. Amer. Meteorol. Soc.* **38**, 283–290.
- Blumen, W., Banta, R. M., Burns, S. P., Fritts, D. C., Newsom, R. K., Poulos, G. S., and Sun, J.: 2001, 'Turbulence Statistics of a Kelvin–Helmholtz Billow Event Observed in the Nighttime Boundary Layer during the CASES-99 Field Program', *Dyn. Atmos. Oceans* **34**, 189–204.
- Bonner, W. D.: 1968, 'Climatology of the Low Level Jet', *Mon. Wea. Rev.* **96**, 833–850.
- Bowen, B. M.: 1996, 'Example of Reduced Turbulence during Thunderstorm Outflows', *J. Appl. Meteorol.* **35**, 1028–1032.
- Browning, K. A. and Wexler, R.: 1968, 'The Determination of Kinematic Properties of a Wind Field Using Doppler Radar', *J. Appl. Meteorol.* **7**, 105–113.
- Coulter, R. L. and Kallistratova, M. A.: 1999, 'The Role of Acoustic Sounding in a High-Technology Era', *Meteorol. Atmos. Phys.* **71**, 3–13.
- Coulter, R. L., Klazura, G., Lesht, B. M., Martin, T. J., Shannon, J. D., Sisterson, D. L., and Wesely, M. L.: 1999, 'The Argonne Boundary Layer Experiments Facility: Using Minisodars to Complement a Wind Profiler Network', *Meteorol. Atmos. Phys.* **71**, 53–59.
- Cuxart, J., Morales, G., Terradellas, E., and Yagüe, C.: 2002, 'Study of Coherent Structures and Estimation of the Pressure Transport Terms for the Nocturnal Stable Boundary Layer', *Boundary-Layer Meteorol.* **105**, 305–328.

- Darby, L. S., Banta, R. M., Brewer, W. A., Neff, W. D., Marchbanks, R. D., McCarty, B. J., Senff, C. J., White, A. B., Angevine, W. M., and Williams, E. J.: 2002, 'Vertical Variations in O<sub>3</sub> Concentrations before and after a Gust Front Passage', *J. Geophys. Res.*, in press.
- Droegemeier, K. K. and Wilhelmson, R. B.: 1987, 'Numerical Simulation of Thunderstorm Outflow Dynamics, Part I: Outflow Sensitivity Experiments and Turbulence Dynamics', *J. Atmos. Sci.* **44**, 1180–1210.
- Eklund, W. L., Carter, D. A., and Balsley, B. B.: 1988, 'A UHF Wind Profiler for the Boundary Layer: Brief Description and Initial Results', *J. Atmos. Oceanic Tech.* **5**, 432–441.
- Frisch, A. S., Orr, B. W., and Martner, B. E.: 1992, 'Doppler Radar Observations of the Development of a Boundary-Layer Nocturnal Jet', *Mon. Wea. Rev.* **120**, 3–16.
- Grund, C. J., Banta, R. M., George, J. L., Howell, J. N., Post, M. J., Richter, R. A., and Weickmann, A. M.: 2001, 'High-Resolution Doppler Lidar for Boundary-Layer and Cloud Research', *J. Atmos. Ocean. Tech.* **18**, 376–393.
- Hoecker, W. L.: 1963, 'Three Southerly Low-Level Jet Systems Delineated by the Weather Bureau Special Pibal Network of 1961', *Mon. Wea. Rev.* **91**, 573–582.
- LeMone, M. A., Grossman, R. L., Coulter, R. L., Wesley, M. L., Klazura, G. E., Poulos, G. S., Blumen, W., Lundquist, J. K., Cuenca, R. H., Kelly, S. F., Brandes, E. A., Oncley, S. P., McMillen, R. T., and Hicks, B. B.: 2000, 'Land-Atmosphere Interaction Research, Early Results, and Opportunities in the Walnut River Watershed in Southeast Kansas: CASES and ABLE', *Bull. Amer. Meteorol. Soc.* **81**, 757–779.
- Lundquist, J. K.: 2000, *The Evening Transition of the Atmospheric Boundary Layer: Inertial Oscillations, and Boundary-Layer Dynamics*, Ph.D. Dissertation, University of Colorado at Boulder, 180 pp.
- Mahrt, L.: 1998, 'Stratified Atmospheric Boundary Layers and Breakdown of Models', *J. Theor. Comp. Fluid Dyn.* **11**, 263–280.
- Mahrt, L.: 1999, 'Stratified Atmospheric Boundary Layers', *Boundary-Layer Meteorol.* **90**, 375–396.
- Mahrt, L. and Vickers, D.: 2002, 'Contrasting Vertical Structures of Nocturnal Boundary Layers', *Boundary-Layer Meteorol.* **105**, 351–363.
- Mitchell, M. J., Arritt, R. W., and Labas, K.: 1995, 'A Climatology of the Warm Season Great Plains Low-Level Jet Using Wind Profiler Observations', *Wea. Forecast.* **10**, 576–591.
- Newsom, R. K. and Banta, R. M.: 2002, 'Shear-Flow Instability in the Stable Nocturnal Boundary Layer as Observed by Doppler Lidar during CASES-99', *J. Atmos. Sci.*, in press.
- Poulos, G. S., Blumen, W., Fritts, D. C., Lundquist, J. K., Sun, J., Burns, S. P., Nappo, C., Banta, R. M., Newsom, R. K., Cuxart, J., Terradellas, E., Balsley, B., and Jensen, M.: 2002, 'CASES-99, A Comprehensive Investigation of the Stable Nocturnal Boundary Layer', *Bull. Amer. Meteorol. Soc.* **83**, 555–581.
- Smedman, A. S.: 1988, 'Observations of a Multi-Level Turbulence Structure in a Very Stable Atmospheric Boundary Layer', *Boundary-Layer Meteorol.* **44**, 231–253.
- Stensrud, D. J.: 1996, 'Importance of Low-Level Jets to Climate: A Review', *J. Climate* **9**, 1698–1711.
- Sun, J., Burns, S. P., Lenschow, D. H., Banta, R., Newsom, R., Coulter, R., Frasier, S., Ince, T., Nappo, C., Cuxart, J., Blumen, W., Lee, X., and Hu, X.-Z.: 2002, 'Intermittent Turbulence Associated with a Density Current Passage in the Stable Boundary Layer', *Boundary-Layer Meteorol.* **105**, 199–219.
- Thorpe, A. J. and Guymer, T. H.: 1977, 'The Nocturnal Jet', *Quart. J. Roy. Meteorol. Soc.* **103**, 633–653.
- Whiteman, C. D., Bian, X., and Zhong, S.: 1997, 'Low-Level Jet Climatology from Enhanced Rawinsonde Observations at a Site in the Southern Great Plains', *J. Appl. Meteorol.* **36**, 1363–1376.
- Wulfmeyer, V. O., Randall, M., Brewer, W. A., and Hardesty R. M.: 2000, '2  $\mu$ m Doppler Lidar Transmitter with High Frequency Stability and Low Chirp', *Opt. Lett.* **25**, 1228–1230.

Zhong, S., Fast, J. D., and Bian, X.: 1996, 'A Case Study of the Great Plains Low-Level Jet Using Wind Profiler Network Data and a High-Resolution Mesoscale Model', *Mon. Wea. Rev.* **124**, 785–806.